HOME

Formation Control For The MAXIM Mission

Richard J. Luquette*

NASA Goddard Space Flight Center, Greenbelt, MD 20771

Jesse Leitner†

NASA Goddard Space Flight Center, Greenbelt, MD 20771

Keith Gendreau‡

NASA Goddard Space Flight Center, Greenbelt, MD 20771

Robert. M. Sanner§

University of Maryland, College Park, MD 20742

Over the next twenty years, a wave of change is occurring in the space-based scientific remote sensing community. While the fundamental limits in the spatial and angular resolution achievable in spacecraft have been reached, based on today's technology, an expansive new technology base has appeared over the past decade in the area of Distributed Space Systems (DSS). A key subset of the DSS technology area is that which covers precision formation flying of space vehicles. Through precision formation flying, the baselines, previously defined by the largest monolithic structure which could fit in the largest launch vehicle fairing, are now virtually unlimited. Several missions including the Micro-Arcsecond X-ray Imaging Mission (MAXIM), and the Stellar Imager will drive the formation flying challenges to achieve unprecedented baselines for high resolution, extended-scene, interferometry in the ultraviolet and X-ray regimes. This paper focuses on establishing the feasibility for the formation control of the MAXIM mission. MAXIM formation flying requirements are on the order of microns, while Stellar Imager mission requirements are on the order of nanometers. This paper specifically addresses: (1) high-level science requirements for these missions and how they evolve into engineering requirements; and (2) the development of linearized equations of relative motion for a formation operating in an n-body gravitational field. Linearized equations of motion provide the ground work for linear formation control designs.

Nomenclature

$\boldsymbol{A}(t)$	=	Dynamics matrix for linearized equations of motion
$\boldsymbol{r}_*$	=	Position vectors, subscripts depicted in figures
$\boldsymbol{u}_{thrust,F}$	=	External control force applied to Follower spacecraft
$\boldsymbol{u}_{thrust,L}$	=	External control force applied to Leader spacecraft
$\boldsymbol{x}$	=	Position of Follower referenced to Leader position
${}^{I}v$	=	Superscript designating inertial (I) frame
μ_i	=	Gravitational parameter for i^{th} body of n-body system
$\|\|\boldsymbol{x}\|\|$	=	The 2-norm of the vector $\boldsymbol{x}$

*Flight Dynamics Analysis Branch, Code 595, Email:rich.luquette@nasa.gov
†GN&C Systems Engineering Branch, Code 591, Email:jesse.leitner@nasa.gov
‡Laboratory for High Energy Physics, Code 662, Email:keith.c.gendreau@nasa.gov
§Aerospace Engineering Department, Email:rmsanner@eng.umd.edu

I. Introduction

Formation flying and DSS missions are becoming the wave of the future for the National Aeronautics and Space Administration and the United States Department of Defense (DoD). Dozens of missions have been formulated, exploiting DSS technologies to enable higher resolution imagery and interferometry, robust and redundant fault-tolerant architectures, and complex networks dispersed over clusters of satellites in space.

One of the most stressing subsets of the proposed collection of DSS missions are those involving precision formation flying, where relative separation and pointing must be maintained (specifically, controlled) to very tight tolerances. A major characteristic in the development of such missions is that the science and engineering elements of the mission design are intertwined in such a way that neither can be performed in an independent or mutually exclusive way. In fact these missions tend to employ formations of "sciencecraft" where each spacecraft is itself a science instrument or a component of a much larger and distributed science instrument, containing a minimum amount of common spacecraft overhead "bus" function. This paper explores the details of developing a control strategy based on mission science requirements with specific reference to the Micro-Arcsecond X-ray Imaging Mission (MAXIM).[1,2]

II. Science to Engineering Requirements Flow Down Process

The seed for a mission concept is a fundamental science goal. The approach to performing the systems engineering is to identify the most fundamental science goal from which some level of engineering can be performed, establish the requirements, allocate the requirements to a general mission architecture, and break these requirements down into basic component level requirements. For example, MAXIM has the most fundamental goal of studying physics in the extreme environment around a black hole - the ultimate endpoint of matter. This provides no information needed to engineer the system. However, a derived requirement is the need to directly image the event horizon around a massive black hole. This can be used to quantify the system requirements. This involves establishing a "resolution" requirement, sizing an aperture

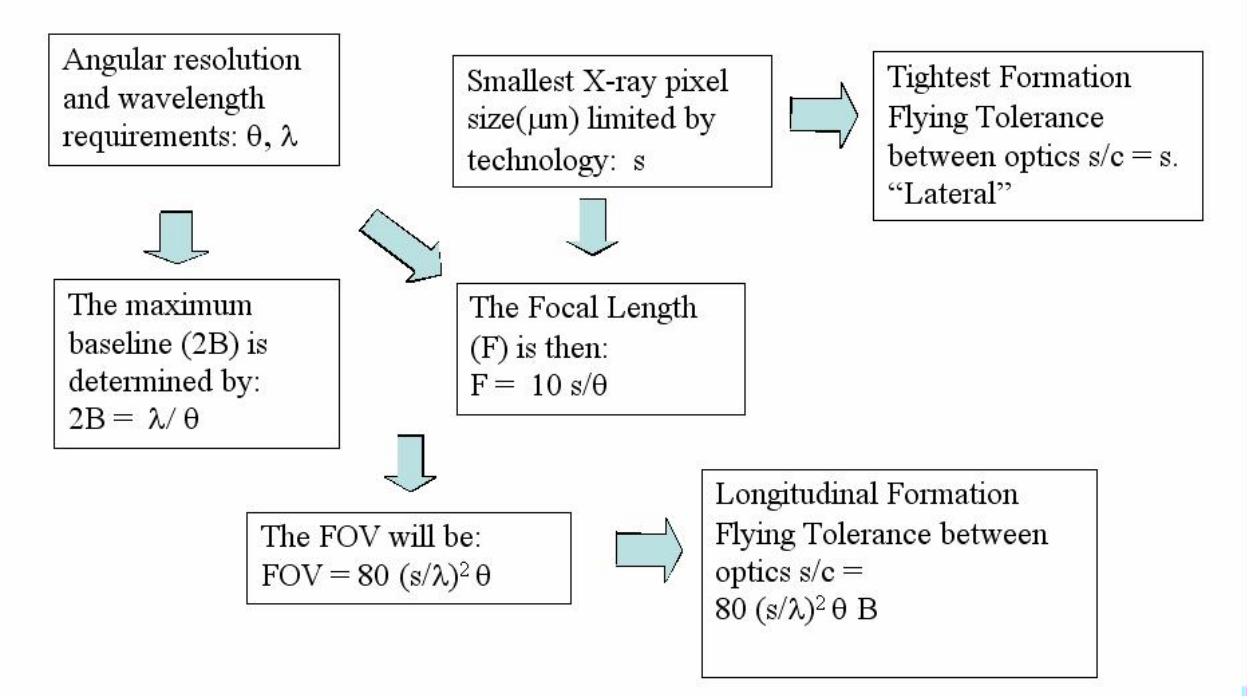

Figure 1. MAXIM Requirements Process Flow

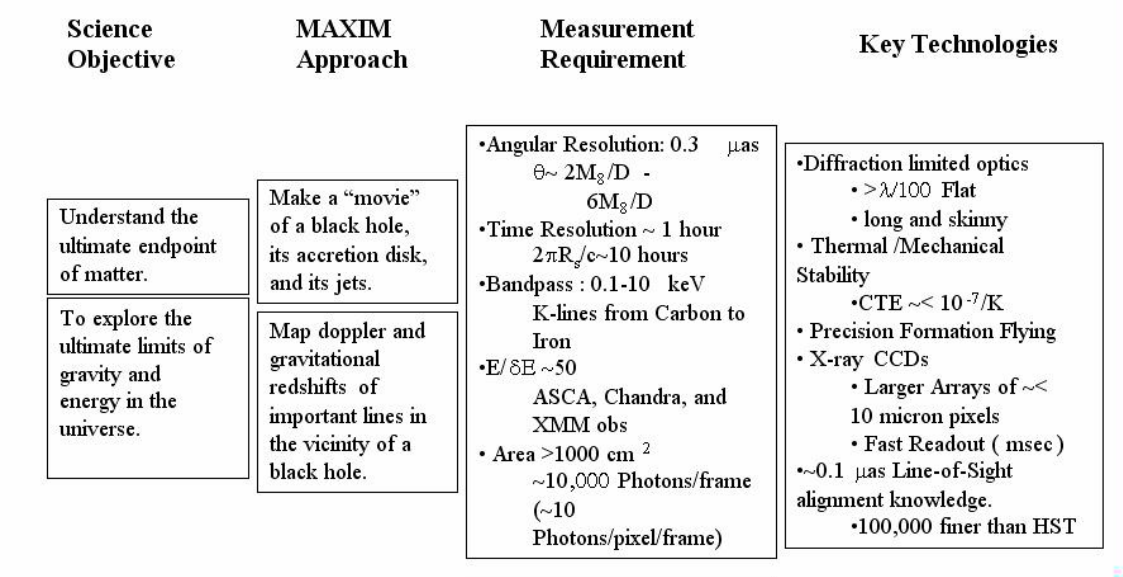

Figure 2. Transition from Science Objectives to High-level Technology Requirements

or system of apertures to meet that requirement, performing a sensitivity analysis to determine tolerances which define performance bounds, and allocating the requirements among the elements of the formation. Also, out of this process falls a formation flying architecture. The requirements at each element must then be allocated to the local systems of the supporting spacecraft or sciencecraft. The requirements should be mapped from the ranges among the loose cluster of spacecraft released from the launch vehicle down to the finest telescope alignment tolerances driven by science. The design process for the formation flying element is a matter of defining a series of sensor and actuator stages with overlapping resolutions and dynamic ranges, including potential stages that account for geometric measurements that are ambiguous when solely using ranging data. For the MAXIM example, the logic flow, partially depicted in Figures 1 and 2, becomes:

1. Science objective: Directly image the event horizon of a black hole

2. Generally, consider the image angular resolution requirement: $\theta = 0.3$ μarcsecond at several mega-parsecs, and from this use the common (approximate) diffraction relationship, $\theta = 1.22\lambda/D$, defined by the Airy disk. For MAXIM, the angular resolution is selected based on the size of the black hole, $\theta = 2M_8/D$, where M_8 is 10^8 solar mass and D is the aperture size. The wavelength, λ, is in the X-Ray band from .2 - 5 nm.

3. The aperture can then be sized accordingly, based on D. For MAXIM, D turns out to be approximately one kilometer, larger than feasible with a monolithic aperture or long booms. If substantial distortion in the aperture were acceptable (e.g., for long wavelengths), then other approaches, such as booms, inflatable membranes, etc., could be considered. A subaperture configuration must be selected.

4. The resolution and field of view requirements fundamentally define the detector size, but qualitatively select a larger size to simplify the problem of finding the target as well as to relieve the formation flying requirements on the detector.

5. The detector area is defined by requirements to

a) collect enough photons to take 10 different snapshots of matter going around the black hole near the Schwartzchild Radius, Rs, such that the integration time $t = Rs/c$ where c is the speed of light ($t \sim 1$ hour), and

b) collect enough photons from an individual element to assist in the overall alignment within a reasonable time scale that avoids engineering problems such as thermal creep, ping, drift, and formation flying issues.

6. Combining the constraints in step 5 above, and starting with a proposed configuration based on previous studies, an optical sensitivity analysis is performed to provide the error budget for each subaperture element

MAXIM Science Requirements	MAXIM Engineering Requirements
θ=1 μas (5×10^{-12} radians) Science	$\Rightarrow$ F=20,000 km
λ=10 Angstroms	$\Rightarrow$ 2B=200m
S=10μm	$\Rightarrow$ FOV = 2.5 arcseconds
	$\Rightarrow$ Long. Control = 700 μm

Figure 3. MAXIM requirements

in fractions of a wavelength. Iterations are performed on the subaperture configuration until one is selected which minimizes the control requirements for the individual segments. At the subatomic distances required for X-ray imaging, independent guidance, navigation and control (GN&C) sensors and actuators cannot provide the measurement and control to meet the instrument requirements. The only option is to use direct information from the detector to determine the errors to correct the image, in the form of wavefront error sensing. The challenges in wavefront sensing for MAXIM will be to collect enough photons to correct the image. Using the dynamic range of the best capability for wavefront control in the X-ray bands, identify a maximum limiting wavefront error that must be achieved from an independent (i.e., not dependent on information from the science instrument) metrology system.

7. The sensitivity analysis from step 6 can also be used to determine a transformation between the wavefront error and the subaperture errors in all six degrees of freedom. The transformation is employed to determine the formation flying requirements that must be met by the independent GN&C system. In conjunction with the aperture configuration (specifically the range between spacecraft), size a laser ranging system based on the requirements above.

8. The laser ranging system can be used for high bandwidth communications as well by modulating information onto the ranging code. However, the dynamic range is very limited, and the system will not be capable of capturing from the initial "lost-in-space" problem, recovering from a large perturbation, not to mention resolving all of the geometric ambiguities of a large formation.

9. The capture range of the laser ranging system defines the performance required of the next sensor, which must also be able to resolve the geometric ambiguities, positioning the spacecraft into shape, at least in a loose form. The concept for this sensor, based on previous efforts in "vision-based navigation" involves placement of a modified star tracker (or simply a charge couple device (CCD) array or active pixel sensor) on a distant detector spacecraft in conjunction with several laser beacons on all of the remaining spacecraft in the formation. This sensor provides relative position (and possibly orientation) measurements of all of the spacecraft as well as the geometric configuration. The dynamic range of this sensor is defined by the size of the CCD array and the focal distance.

10. A coarse radio frequency (RF) system is defined for operations between the worst case, lost-in-space condition and the field-of-view of the CCD formation sensor. Additionally, this system is required for general constellation housekeeping, failure recovery, and collision avoidance.

The requirements for MAXIM are summarized in figure 3.

The requirements flow process implies an inherent sensing and metrology concept for similar large aperture imaging formations. Associated with each of the matches in sensor dynamic ranges and resolutions above is an analogous series of actuation systems, which in combination define the formation flying architecture. Because the suite of actuators is not as diverse as the suite of sensors, the details will not be addressed in this paper, other than to say that for many of the precision formation flying missions, they will consist of a nested series of low-thrust, high specific impulse (Isp) devices with overlapping dynamic ranges and resolutions.

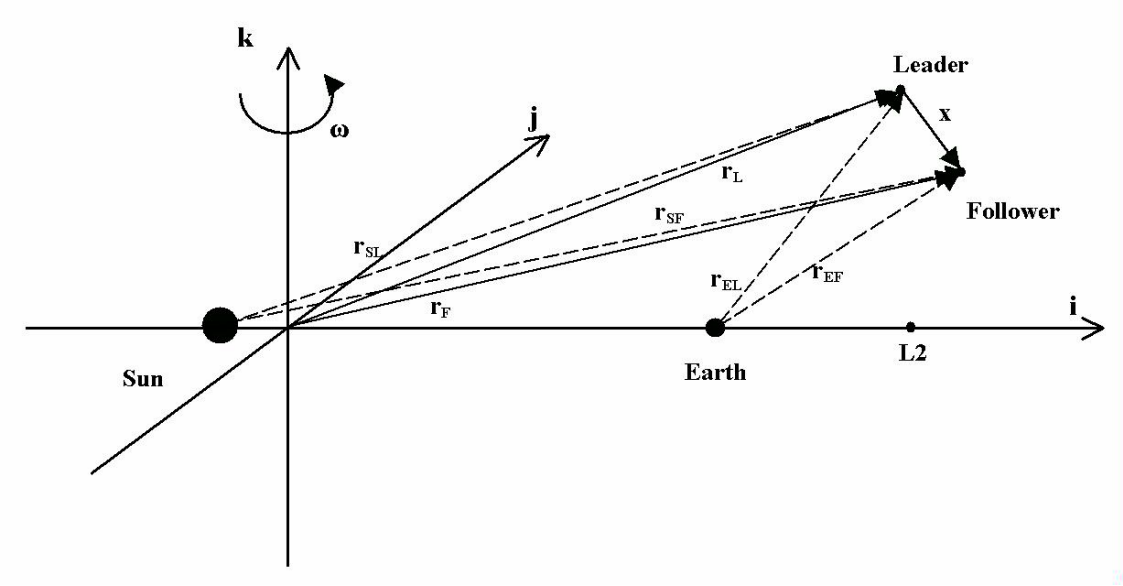

Figure 4. Two Spacecraft Orbiting in the Earth/Moon - Sun Rotating Frame

III. Formation Control

A. Prior Work

Achieving the precision formation flying requirements for the MAXIM mission poses significant technical challenges within the areas of metrology and control law design. In particular, the requirement for 10 micron control in the radial direction provides immense design challenges in the metrology, the control actuators, and the control algorithms. Each of these issues presents unique challenges. Earlier works explored nonlinear control strategies to address the problem.[3,4] This paper focuses on the issue of control design, specifically linear control strategies. Development of a linear controller requires a linearized form of the relative dynamics of a spacecraft relative to a reference trajectory. Figure 4 depicts a spacecraft operating in the vicinity of the L_2 point of Earth/Moon-Sun libration point. Modelling the Earth/Moon as a single mass, the linearized dynamics of a Follower spacecraft relative to a Leader are expressed in inertial coordinates as[5]

$$\dot{\boldsymbol{\xi}} \;\; = {}^{\mathrm{I}}\mathbf{A}(t)\,\boldsymbol{\xi} \; + \boldsymbol{B}\,(\boldsymbol{u}_{thrust,F} - \boldsymbol{u}_{thrust,L}) \tag{1}$$

Where:

$$\boldsymbol{\xi} = \begin{bmatrix} \boldsymbol{x} \\ \dot{\boldsymbol{x}} \end{bmatrix}; \quad {}^{\mathrm{I}}\mathbf{A}(t) = \begin{bmatrix} \mathbf{0} & \mathbf{I_3} \\ {}^{I}\boldsymbol{\Xi}(t) & \mathbf{0} \end{bmatrix}; \quad \boldsymbol{B} = \begin{bmatrix} \mathbf{0} \\ \mathbf{I_3} \end{bmatrix}$$

$$\begin{aligned} {}^{I}\boldsymbol{\Xi}(t) \;\; &= \left\{-(c_1 + c_2)\,\mathbf{I_3} + 3\,c_1\,[\mathring{\boldsymbol{r}}_{\boldsymbol{EL}}(t)\,\mathring{\boldsymbol{r}}_{\boldsymbol{EL}}(t)^{\mathsf{T}}] + 3\,c_2\,[\mathring{\boldsymbol{r}}_{\boldsymbol{SL}}(t)\,\mathring{\boldsymbol{r}}_{\boldsymbol{SL}}(t)^{\mathsf{T}}]\right\} \\ \\ c_1 \;\; &= \mu_{em}||\boldsymbol{r}_{\boldsymbol{EL}}||^{-3} \\ c_2 \;\; &= \mu_s||\boldsymbol{r}_{\boldsymbol{SL}}||^{-3} \end{aligned}$$

This expression does not require the formation to be in the vicinity of a libration point. In the remainder of this paper the linearized dynamics are generalized for the n-body problem.

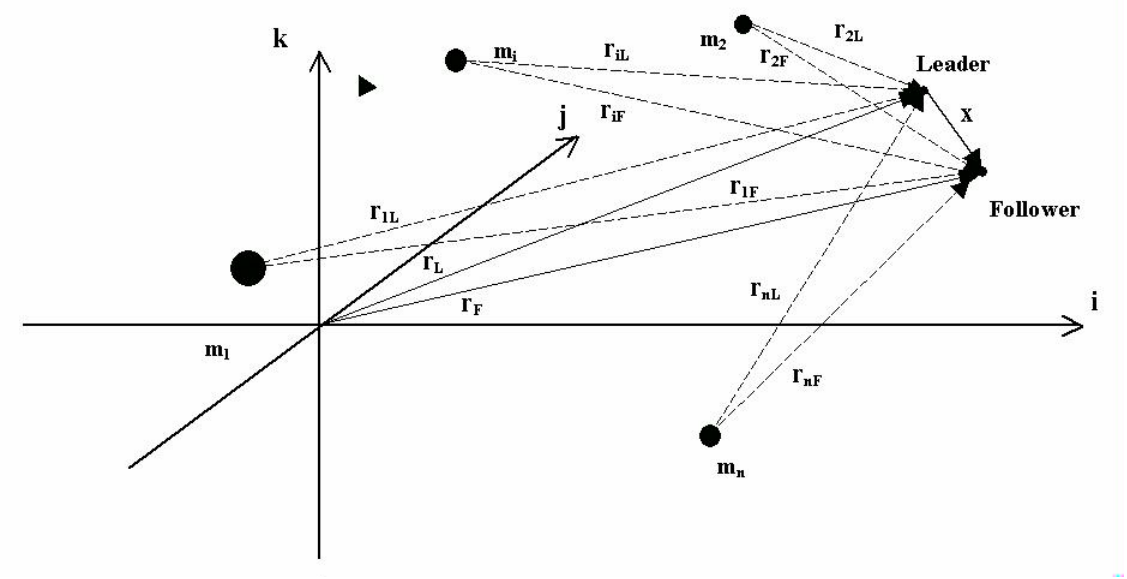

Figure 5. Two Spacecraft Under the Gravitational Influence of n-Bodies

B. Dynamics of Relative Motion for the n-Body Problem

The n-body problem examines the behavior of an infinitesimal mass in the combined gravitational field of 'n' finite masses orbiting their common center of mass. A typical two spacecraft formation operating in the gravitational field of n-bodies as shown in figure 5

Treating each body as a point mass, the equation of motion for the Leader and Follower spacecraft are Leader:

$$\ddot{\boldsymbol{r}}_{_L} = -\mu_1 \frac{\boldsymbol{r}_{1L}}{||\boldsymbol{r}_{1L}||^3} - \mu_2 \frac{\boldsymbol{r}_{2L}}{||\boldsymbol{r}_{2L}||^3} - ... - \mu_i \frac{\boldsymbol{r}_{iL}}{||\boldsymbol{r}_{iL}||^3} - ... - \mu_n \frac{\boldsymbol{r}_{nL}}{||\boldsymbol{r}_{nL}||^3} + \boldsymbol{u}_{thrust,L} \tag{2}$$

Follower:

$$\ddot{\boldsymbol{r}}_{_F} = -\mu_1 \frac{\boldsymbol{r}_{1F}}{||\boldsymbol{r}_{1F}||^3} - \mu_2 \frac{\boldsymbol{r}_{2F}}{||\boldsymbol{r}_{2F}||^3} - ... - \mu_i \frac{\boldsymbol{r}_{iF}}{||\boldsymbol{r}_{iF}||^3} - ... - \mu_n \frac{\boldsymbol{r}_{nF}}{||\boldsymbol{r}_{nF}||^3} + \boldsymbol{u}_{thrust,F} \tag{3}$$

Differencing eqs. (2) and (3) yields the relative motion of the Follower with respect to the Leader:

$$\begin{aligned} \ddot{\boldsymbol{x}} &= \ddot{\boldsymbol{r}}_{_F} - \ddot{\boldsymbol{r}}_{_L} \\ &= -\sum_{i=1}^{n} \mu_i \frac{\boldsymbol{r}_{iF}}{||\boldsymbol{r}_{iF}||^3} + \boldsymbol{u}_{thrust,F} - (-\sum_{i=1}^{n} \mu_i \frac{\boldsymbol{r}_{iL}}{||\boldsymbol{r}_{iL}||^3} + \boldsymbol{u}_{thrust,L}) \\ &= -\left\{ \sum_{i=1}^{n} \frac{\mu_i}{||\boldsymbol{r}_{iF}||^3} \right\} \boldsymbol{x} - \sum_{i=1}^{n} \mu_i \left\{ \frac{1}{||\boldsymbol{r}_{iF}||^3} - \frac{1}{||\boldsymbol{r}_{iL}||^3} \right\} \boldsymbol{r}_{iL} + (\boldsymbol{u}_{thrust,F} - \boldsymbol{u}_{thrust,L}) \end{aligned} \tag{4}$$

Eq. (4) provides an exact expression of the nonlinear dynamics of relative motion between the Follower and Leader spacecraft. The next step is to linearize the relative dynamics of the Follower with respect to the Leader.

C. Linearized Dynamics

The approach to linearizing eq. 4 is to examine each term. Consider $\left\{\frac{1}{||\boldsymbol{r}_{iF}||^3} - \frac{1}{||\boldsymbol{r}_{iL}||^3}\right\}$

$$\begin{aligned}\left\{\frac{1}{||\boldsymbol{r}_{iF}||^3} - \frac{1}{||\boldsymbol{r}_{iL}||^3}\right\} &= \left\{\frac{1}{||\boldsymbol{r}_{iL}+\boldsymbol{x}||^3} - \frac{1}{||\boldsymbol{r}_{iL}||^3}\right\} \\ &= \left\{\frac{1}{[(\boldsymbol{r}_{iL}+\boldsymbol{x})^{\mathsf{T}}(\boldsymbol{r}_{iL}+\boldsymbol{x})]^{3/2}} - \frac{1}{||\boldsymbol{r}_{iL}||^3}\right\} \\ &= \left\{\left[||\boldsymbol{r}_{iL}||^2 + \boldsymbol{x}^{\mathsf{T}}\boldsymbol{x} + 2\,(\boldsymbol{r}_{iL}{}^{\mathsf{T}}\boldsymbol{x})\right]^{-3/2} - ||\boldsymbol{r}_{iL}||^{-3}\right\} \\ &= \left\{\left[1 + \frac{\boldsymbol{x}^{\mathsf{T}}\boldsymbol{x}}{||\boldsymbol{r}_{iL}||^2} + 2\,\frac{(\boldsymbol{r}_{iL}{}^{\mathsf{T}}\boldsymbol{x})}{||\boldsymbol{r}_{iL}||^2}\right]^{-3/2} - 1\right\}||\boldsymbol{r}_{iL}||^{-3}\end{aligned} \tag{5}$$

Apply a binomial expansion to first order, resulting in

$$\begin{aligned}\left\{\frac{1}{||\boldsymbol{r}_{iF}||^3} - \frac{1}{||\boldsymbol{r}_{iL}||^3}\right\} &= \left\{\left[1 + \frac{\boldsymbol{x}^{\mathsf{T}}\boldsymbol{x}}{||\boldsymbol{r}_{iL}||^2} + 2\,\frac{(\boldsymbol{r}_{iL}{}^{\mathsf{T}}\boldsymbol{x})}{||\boldsymbol{r}_{iL}||^2}\right]^{-3/2} - 1\right\}||\boldsymbol{r}_{iL}||^{-3} \\ &= \left\{\left[1 + (-\tfrac{3}{2})\left(\frac{\boldsymbol{x}^{\mathsf{T}}\boldsymbol{x}}{||\boldsymbol{r}_{iL}||^2} + 2\,\frac{(\boldsymbol{r}_{iL}{}^{\mathsf{T}}\boldsymbol{x})}{||\boldsymbol{r}_{iL}||^2}\right) + H.O.T.\right] - 1\right\}||\boldsymbol{r}_{iL}||^{-3} \\ &\approx -\tfrac{3}{2}\,\left(\frac{\boldsymbol{x}^{\mathsf{T}}\boldsymbol{x}}{||\boldsymbol{r}_{iL}||^2} + 2\,\frac{(\boldsymbol{r}_{iL}{}^{\mathsf{T}}\boldsymbol{x})}{||\boldsymbol{r}_{iL}||^2}\right)||\boldsymbol{r}_{iL}||^{-3}\end{aligned} \tag{6}$$

It follows from Eq. 6 that

$$\sum_{i=1}^{n}\frac{\mu_i}{||\boldsymbol{r}_{iF}||^3} \approx \sum_{i=1}^{n}\frac{\mu_i}{||\boldsymbol{r}_{iL}||^3}\left(1 - \tfrac{3}{2}\frac{\boldsymbol{x}^{\mathsf{T}}\boldsymbol{x}}{||\boldsymbol{r}_{iL}||^2} - 3\,\frac{(\boldsymbol{r}_{iL}{}^{\mathsf{T}}\boldsymbol{x})}{||\boldsymbol{r}_{iL}||^2}\right) \tag{7}$$

Substituting Eqs. 6 and 7 into Eq. 4 gives

$$\begin{aligned}\ddot{\boldsymbol{x}} \approx &-\left\{\sum_{i=1}^{n}\frac{\mu_i}{||\boldsymbol{r}_{iL}||^3}\left(1 - \tfrac{3}{2}\frac{\boldsymbol{x}^{\mathsf{T}}\boldsymbol{x}}{||\boldsymbol{r}_{iL}||^2} - 3\,\frac{(\boldsymbol{r}_{iL}{}^{\mathsf{T}}\boldsymbol{x})}{||\boldsymbol{r}_{iL}||^2}\right)\right\}\,\boldsymbol{x} + \sum_{i=1}^{n}\left\{\frac{\mu_i}{||\boldsymbol{r}_{iL}||^5}\left(\tfrac{3}{2}\boldsymbol{x}^{\mathsf{T}}\boldsymbol{x} + 3\,\boldsymbol{r}_{iL}{}^{\mathsf{T}}\boldsymbol{x}\right)\boldsymbol{r}_{iL}\right\} \\ &+(\boldsymbol{u}_{thrust,F} - \boldsymbol{u}_{thrust,L})\end{aligned} \tag{8}$$

Replace $(\boldsymbol{x}^{\mathsf{T}}\boldsymbol{x})\,\boldsymbol{r}_{iL}$ and $(\boldsymbol{r}_{iL}{}^{\mathsf{T}}\boldsymbol{x})\,\boldsymbol{r}_{iL}$ in Eq. 8 with the equivalent expressions, $(\boldsymbol{r}_{iL}\,\boldsymbol{x}^{\mathsf{T}})\boldsymbol{x}$ and $(\boldsymbol{r}_{iL}\,\boldsymbol{r}_{iL}{}^{\mathsf{T}})\boldsymbol{x}$, yielding

$$\begin{aligned}\ddot{\boldsymbol{x}} &\approx -\left\{\sum_{i=1}^{n}\frac{\mu_i}{||\boldsymbol{r}_{iL}||^3}\left(1 - \tfrac{3}{2}\frac{\boldsymbol{x}^{\mathsf{T}}\boldsymbol{x}}{||\boldsymbol{r}_{iL}||^2} - 3\,\frac{(\boldsymbol{r}_{iL}{}^{\mathsf{T}}\boldsymbol{x})}{||\boldsymbol{r}_{iL}||^2}\right)\right\}\,\boldsymbol{x} + \sum_{i=1}^{n}\left\{\frac{\mu_i}{||\boldsymbol{r}_{iL}||^5}\left(\tfrac{3}{2}\boldsymbol{r}_{iL}\,\boldsymbol{x}^{\mathsf{T}} + 3\,\boldsymbol{r}_{iL}\,\boldsymbol{r}_{iL}{}^{\mathsf{T}}\right)\boldsymbol{x}\right\} \\ &+(\boldsymbol{u}_{thrust,F} - \boldsymbol{u}_{thrust,L}) \\ &= \left\{-\sum_{i=1}^{n}\frac{\mu_i}{||\boldsymbol{r}_{iL}||^3}\left[\left(1 - \tfrac{3}{2}\frac{\boldsymbol{x}^{\mathsf{T}}\boldsymbol{x}}{||\boldsymbol{r}_{iL}||^2} - 3\,\frac{(\boldsymbol{r}_{iL}{}^{\mathsf{T}}\boldsymbol{x})}{||\boldsymbol{r}_{iL}||^2}\right)\mathbf{I_3} - \frac{1}{||\boldsymbol{r}_{iL}||^2}\left(\tfrac{3}{2}\boldsymbol{r}_{iL}\,\boldsymbol{x}^{\mathsf{T}} + 3\,\boldsymbol{r}_{iL}\,\boldsymbol{r}_{iL}{}^{\mathsf{T}}\right)\right]\right\}\,\boldsymbol{x} \\ &+(\boldsymbol{u}_{thrust,F} - \boldsymbol{u}_{thrust,L})\end{aligned} \tag{9}$$

In order to remove the state dependence of the dynamics matrix in Eq. 9. assume a tight formation with $||\boldsymbol{x}|| << ||\boldsymbol{r}_{iL}||$, for all i. Thus, $||-\frac{3}{2}\frac{\boldsymbol{x}^{\mathsf{T}}\boldsymbol{x}}{||\boldsymbol{r}_{iL}||^2} - 3\,\frac{(\boldsymbol{r}_{iL}{}^{\mathsf{T}}\boldsymbol{x})}{||\boldsymbol{r}_{iL}||^2}|| << 1$. Likewise, the term $\frac{3}{2}\frac{\boldsymbol{r}_{iL}\,\boldsymbol{x}^{\mathsf{T}}}{||\boldsymbol{r}_{iL}||^2}$ is also neglected, since its matrix norm is much smaller than the remaining terms,. Eq. 9 simplifies to

$$\begin{aligned} \ddot{\boldsymbol{x}} &= -\left\{ \sum_{i=1}^{n} \frac{\mu_i}{||\boldsymbol{r}_{iL}||^3} \left[\mathbf{I_3} - \frac{3}{||\boldsymbol{r}_{iL}||^2} \left(\boldsymbol{r}_{iL}\ \boldsymbol{r}_{iL}{}^{\mathsf{T}} \right) \right] \right\} \boldsymbol{x} + \left(\boldsymbol{u}_{thrust,F} - \boldsymbol{u}_{thrust,L} \right) \\ &= -\left\{ \sum_{i=1}^{n} \frac{\mu_i}{||\boldsymbol{r}_{iL}||^3} \left[\mathbf{I_3} - 3 \left(\mathring{\boldsymbol{r}}_{iL}\ \mathring{\boldsymbol{r}}_{iL}{}^{\mathsf{T}} \right) \right] \right\} \boldsymbol{x} + \left(\boldsymbol{u}_{thrust,F} - \boldsymbol{u}_{thrust,L} \right) \end{aligned} \tag{10}$$

Note that $\mathring{\boldsymbol{r}}_{iL}$ denotes a unit vector along $\boldsymbol{r}_{iL}$.

In summary the linearized dynamics are expressed as

$$\ddot{\boldsymbol{x}} = {}^{I}\boldsymbol{\Xi}(t)\, \boldsymbol{x} + \boldsymbol{u}_{thrust,F} - \boldsymbol{u}_{thrust,L} \tag{11}$$

where

$${}^{I}\boldsymbol{\Xi}(t) = -\sum_{i=1}^{n} \frac{\mu_i}{||\boldsymbol{r}_{iL}||^3} \left[\mathbf{I_3} - 3 \left(\mathring{\boldsymbol{r}}_{iL}\ \mathring{\boldsymbol{r}}_{iL}{}^{\mathsf{T}} \right) \right]$$

The linearized dynamics in matrix form are

$$\dot{\boldsymbol{\xi}} = {}^{\mathrm{I}}\mathbf{A}(t)\, \boldsymbol{\xi} + \boldsymbol{B}\, \left(\boldsymbol{u}_{thrust,F} - \boldsymbol{u}_{thrust,L} \right) \tag{12}$$

Where:

$$\boldsymbol{\xi} = \begin{bmatrix} \boldsymbol{x} \\ \dot{\boldsymbol{x}} \end{bmatrix}; \quad {}^{\mathrm{I}}\mathbf{A}(t) = \begin{bmatrix} \mathbf{0} & \mathbf{I_3} \\ {}^{I}\boldsymbol{\Xi}(t) & \mathbf{0} \end{bmatrix}; \quad \boldsymbol{B} = \begin{bmatrix} \mathbf{0} \\ \mathbf{I_3} \end{bmatrix}$$

IV. Conclusions

The process for systems engineering and technology planning for precision formation flying missions is fully entwined with the science definition and instrument design. The MAXIM mission is used as an evidential example in this paper. After laying out engineering and technology requirements, one small, but challenging element of the engineering problem, that of controlling a formation near the Earth-Sun L2 point, is discussed.

Linear control design is attractive for many applications, based on heritage. Linear control theory offers many analysis tools for characterizing control performance. This paper presents the linearized dynamics of relative motion for two spacecraft operating under the influence of an n-body gravitational field. The linearized dynamics form the basis for a good linear control design.

Future work will employ the linearized dynamics in various control designs. This work will include consideration of spacecraft attitude, disturbances due to differential solar pressure, and measurement error/noise.

V. Acknowledgement

This work was funded under the Revolutionary Spacecraft Systems Project in the Mission and Science Measurement theme in NASA headquarters.

References

[1]Gendreau, K. C. and Cash, W. C. and Shipley, A. F. and White, N., "MAXIM X-Ray Interferometry Mission," *Proceedings of SPIE Optics for EUV, X-Ray, and Gamma Ray Astronomy Conference*, San Diego, CA, August 2003.

[2]Gendreau, K. C. and Leitner, J. and Markley, L. and Cash, W. C. and Shipley, A. F., "Requirements and Options for a Stable Inertial Reference Frame for a 100 μarcsecond Imaging Telescope," *SPIE's X-Ray and Gamma-Ray Telescopes and Instruments for Astronomy Conference*, Waikoloa, Hawaii, August 2002.

[3]Luquette, R. J. and Sanner, R. M., "A Nonlinear Approach to Spacecraft Formation Control in the Vicinity of a Collinear Libration Point," *Proceedings of the AAS/AIAA Astrodynamics Specialist Conference*, July 2001, Paper No. AAS 01-330.

[4]Luquette, R. J. and Sanner, R. M., "A Nonlinear, Six-Degree of Freedom, Precision Formation Control Algorithm, Based on Restricted Three Body Dynamics," *26th Annual AAS Guidance and Control Conference*, February 2003, Paper No. AAS 03-007.

[5]Luquette, R. J. and Sanner, R. M., "Linear State-Space Representation of the Dynamics of Relative Motion, Based on Restricted Three Body Dynamics," *AIAA Guidance and Control Conference*, August 2004, Paper No. AIAA-2004-4783.